Research Article | Vol. 2, No. 11 / 15 November 2019 / OSA Continuum 3019
OSA CONTINUUM

3D printed lens for depth of field imaging

KELLI C. KIEKENS[1] AND JENNIFER K. BARTON[2,*]

[1] College of Optical Science, University of Arizona, Tucson, AZ 85719, USA
[2] Biomedical Engineering, University of Arizona, Tucson, AZ 85721, USA
[*] barton@email.arizona.edu
http://bmeoptics.engr.arizona.edu/

Abstract: This manuscript presents design considerations and testing of a 3D printed lens with an outer diameter of 0.5mm. Off-the-shelf GRIN and half-ball lenses with the same outer diameter were used to compare the angular field of view and resolution at object distances between 5mm and 100mm. Results show the performance of this 3D printed optic is between that of the half-ball lens and the GRIN lens with the possibility for improvement. This opens opportunities in the sub-millimeter, refractive optics space. Our goal is to utilize 3D printed lenses in a sub-millimeter diameter endoscope for *in vivo* imaging.

© 2019 Optical Society of America under the terms of the OSA Open Access Publishing Agreement

1. Introduction

In the effort to miniaturize endoscopes to sub-millimeter size for medical purposes, optical components must also be miniaturized. Off-the-shelf lenses small enough for this application are currently limited to gradient index (GRIN), half-ball, and ball lenses. Custom lenses on this scale are very expensive as only a few manufacturers are willing to make them. They can also have very long lead times and low yield from a manufacturer's point of view. Lens designs requiring alignment of 2 or more lenses becomes increasingly difficult on the micro scale.

Many methods are currently being researched for fabrication of micro-lens arrays [1–3], but very few methods are available for single refractive lenses at the sub-millimeter scale. In the past, micro-machining was investigated as a way to create and align sub millimeter diffractive elements [4]. Inkjet printing of micro-lenses has been shown to create lenses directly on the tips of optical fibers [5]. Inkjet printing technology has also been used to create lenses used for smartphone microscopy [6]. However, this process is limited to plano-convex spherical shapes. Injection molding has a costly setup expense making it too expensive for prototyping or small batch manufacturing and is limited in the shapes and sizes that can be produced. Mold shrinkage can cause the final product shape to deviate from the design shape in unpredictable ways [7].

3D printed optics have the advantage of being customizable in shape and size, speed from design to physical part, and the potential for ease of multi-element alignment. Lenses have been 3D printed using similar technology for single plane imaging [8], multiple lens elements [9], and freeform optics [10].

The objective of this study was to compare a simple 3D printed optic against off-the-shelf parts. The comparison parameters were the angular field of view (FOV) and resolution over a depth of field from 5mm to 100mm without adjusting focus for image quality at each object location. This depth of field was chosen to match the performance of current endoscopes.

2. Lens manufacturing design constraints

For this study, the Photonic Professional GT (Nanoscribe, Karsruhe, Germany) was used to print the optic in IP-S resin (Nanoscribe). The printing was performed with a 25x objective to ensure a printing field of view large enough to avoid stitching of the print. A drop of resin was placed on a glass slide and a laser was focused onto a small area to polymerize the resin via 2-photon absorption. The laser was scanned in x and y using piezo-electric devices then incremented in z

#379666 https://doi.org/10.1364/OSAC.2.003019
Journal © 2019 Received 3 Oct 2019; accepted 6 Oct 2019; published 17 Oct 2019

OSA CONTINUUM

to build the full structure. Due to this print process, a flat surface needed to be incorporated into the design to adhere to the glass slide. We designed a plano-convex lens so that the planar side could be printed directly on the slide. A thin annular stand could be integrated into the design for an optic with two curved surfaces.

The print area for the optic was limited to approximately 0.7mm by the microscope objective. The smallest off-the-shelf ball or half-ball lenses found online were 0.5mm. A fused silica half-ball lens and a GRIN lens with outer diameters of 0.5mm were purchased for comparison to the 3D printed lens (PN: 64-515 and 67-390, Edmund Optics, Barrington, NJ, USA). For a direct comparison of the 3D printed optic to the selected off-the-shelf components, the design was constrained to a 0.5mm outer diameter.

3. Optical modeling

A new material was added to the material library in OpticStudio (Zemax, Kirkland, Washington, USA) using information from the manufacturer for a dispersion curve of the resin. Using the multi-configuration editor, object distances were set to 5mm, 20mm, 50mm, and 100mm with weights of 100, 100, 10 and 1 respectively. This weighting provided the best resolution images for close objects while maintaining acceptable image quality further away. The back focal distance remained constant for all object distances. In the case of an endoscope, image distance would not be adjustable, and objects at all distances would need to be visible simultaneously. The software optimized for RMS spot size using radius of curvature and conic constant of the front surface, thickness of the lens, and back focal distance as optimization parameters.

OpticStudio files were downloaded directly from the Edmund Optics website for the GRIN lens and half-ball lens. A multi-configuration editor was set up with the same 4 object distances with the same weight as was done when designing the 3D printed lens. For both of these lenses, the back focal distance was the only variable while remaining the same distance foe each object distance. The theoretical performance of all lenses after optimization was compared. Fig. 1.(A) shows the theoretical on axis modulation transfer function (MTF) for each of the 3 lenses at the 20mm object distance. Fig. 1.(B) shows the theoretical 15° off axis tangential and sagittal MTF for each of the three lenses at a 20mm object distance.

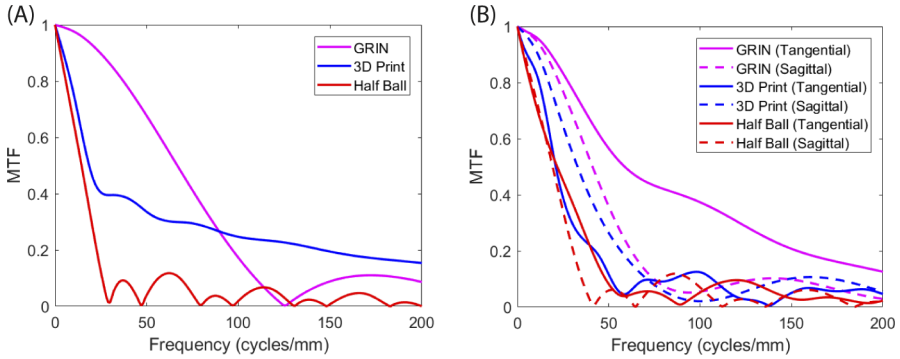

Fig. 1. (A) The theoretical MTF on axis at a 20mm object distance for a GRIN lens, the 3D printed lens, and a fused silica half-ball lens. (B) Theoretical tangential and sagittal MTF for the 15° field of view for the same three lenses.

From the graphs, the performance of the 3D printed lens was anticipated to be between that of the half-ball lens and the GRIN lens at the 20mm object distance. A similar relationship held for each of the object distances.

OSA CONTINUUM

4. Experimental setup

A glass 2" x 2" negative, 1951 USAF Resolution Target (PN: 38-256, Edmund Optics) was held in a custom lens holder and stand at distances of 5mm, 20mm, 50mm, and 100mm away from the front surface of the lens. The lens holder and stand were positioned within a microscope stage so that there was fine control over the z-axis to find the focus position.

The resolution target was placed at the 20mm object distance in a transillumination setup using a broadband white light source (PN: 59-235, Edmund Optics). For resolution testing, images were acquired using a 40x infinity corrected microscope objective (PN: UAPON40XW340, Olympus, Tokyo, Japan) focused onto the image formed by the lens being tested. A 150mm focal length lens then focused a magnified image on a PIXIS 1024 CCD detector (Princeton Instruments, Trenton, NJ,USA) and the WinView software was used to display the image. The microscope stage height was adjusted to the position of the smallest resolvable element as determined by visibly separate peaks when using the intensity cross-section tool.

Without adjusting focus, the resolution target was moved to the 100mm object distance and an image was acquired. The target was subsequently moved to the 50mm, 20mm, then 5mm object distances acquiring images at each location. At the 20mm object distance the cross section intensity was used to ensure the same performance as when the focus position was determined. This confirmed nothing moved during acquisition of images at the 100mm and 50mm object distances. The camera exposure time was kept constant at all distances.

The objective was changed to a 20x objective (PN: UAPON20XW340, Olympus) so that the FOV could be determined. Because the 20x and 40x objectives had different working distances, best focus at the 20mm distance was found again. A Ronchi ruling with 25 lp/inch replaced the resolution target at the 20mm location and an image was acquire for the FOV measurement.

Once all images were collected for one lens, a different lens was placed in the lens holder and the process repeated until all depth of field and FOV images were collected for each of the three lenses.

5. Results

The quality of the actual 3D print shape compared to the design shape is first presented. Then the images from each lens at various object distances are shown and a summary of resolution and field of view of the lenses are tabulated.

5.1. Print quality

Figure 2 shows a side by side visual comparison of an image of the printed lens taken with an Olympus microscope (PN: BX41, Olympus) with a 4x objective (PN: PLN4X, Olympus) along with the Soldiworks model of the lens.

The designed convex surface of the 3D printed lens had a radius of curvature of .233mm and a conic constant of −0.890. The surface can be described by the SAG equation [11]:

$$Sag = -\frac{cr^2}{1+\sqrt{1-(1+k)c^2r^2}}\,. \tag{1}$$

Here, r is the distance from the optical axis, c is the curvature of the lens surface and k is the conic constant.

A NewView 3D Optical Surface Profiler (Zygo, Middlefield, CT, USA) was used to measure the surface shape (Fig. 3). A cross section of the data was imported into MatLab (MathWorks, Natick, MA, USA) and plotted along with the equation describing the design shape (Fig. 4(A)). The ideal shape was then subtracted from the measured data (Fig. 4(B)) and the RMS of this data was calculated. The difference data give a total shape RMS error of 595.5nm.

OSA CONTINUUM

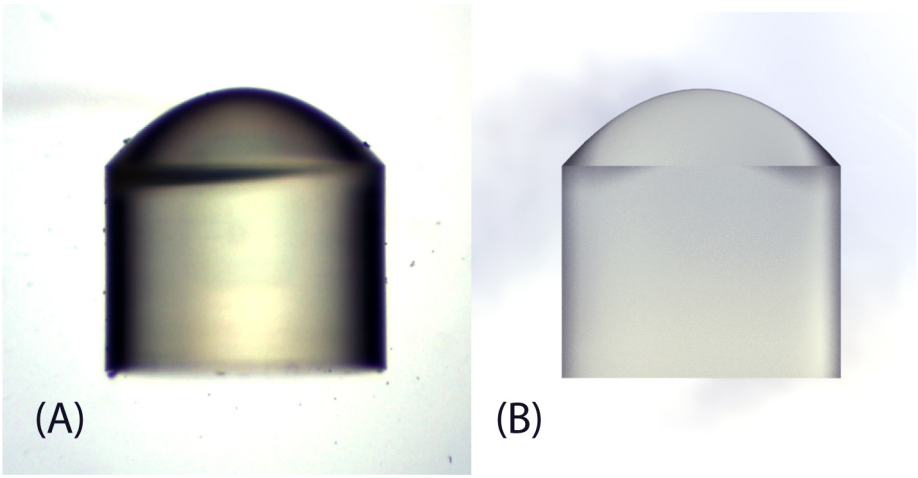

Fig. 2. (A) Image of the 3D printed lens with a 4x objective. (B) 3D render of the prescribed lens in Solidworks.

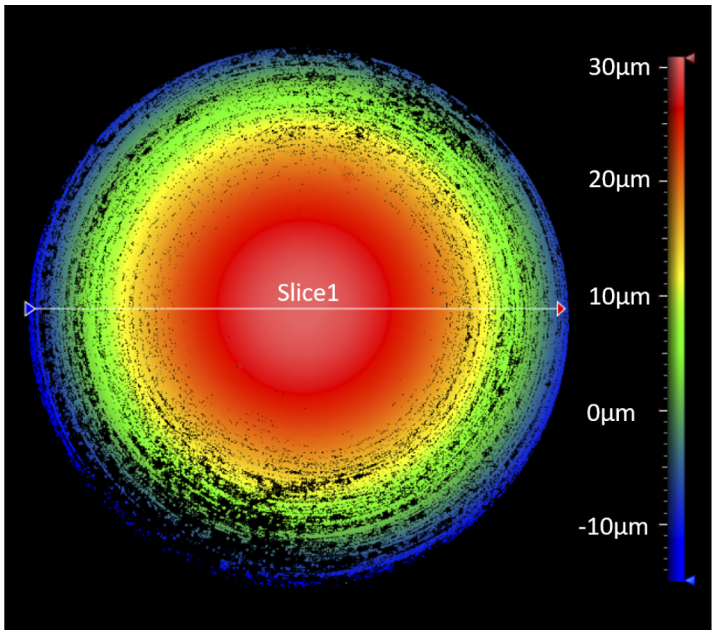

Fig. 3. Surface profile of the 3D printed lens as measured by the NewView 3D Optical Surface Profiler. The data points from slice 1 were used to compare to the ideal shape.

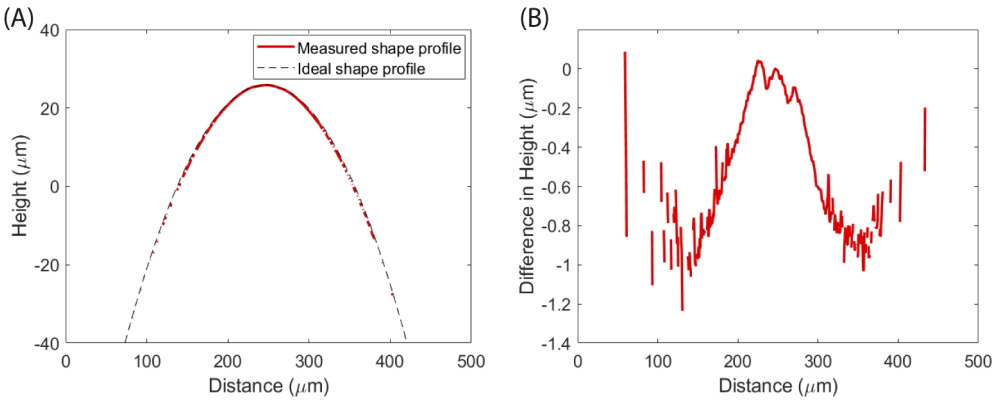

Fig. 4. (A) Cross section of measured data from the NewView Profiler plotted with the designed surface shape. (B) Design shape subtracted from the measured data. The calculated RMS total shape error is 595.5nm.

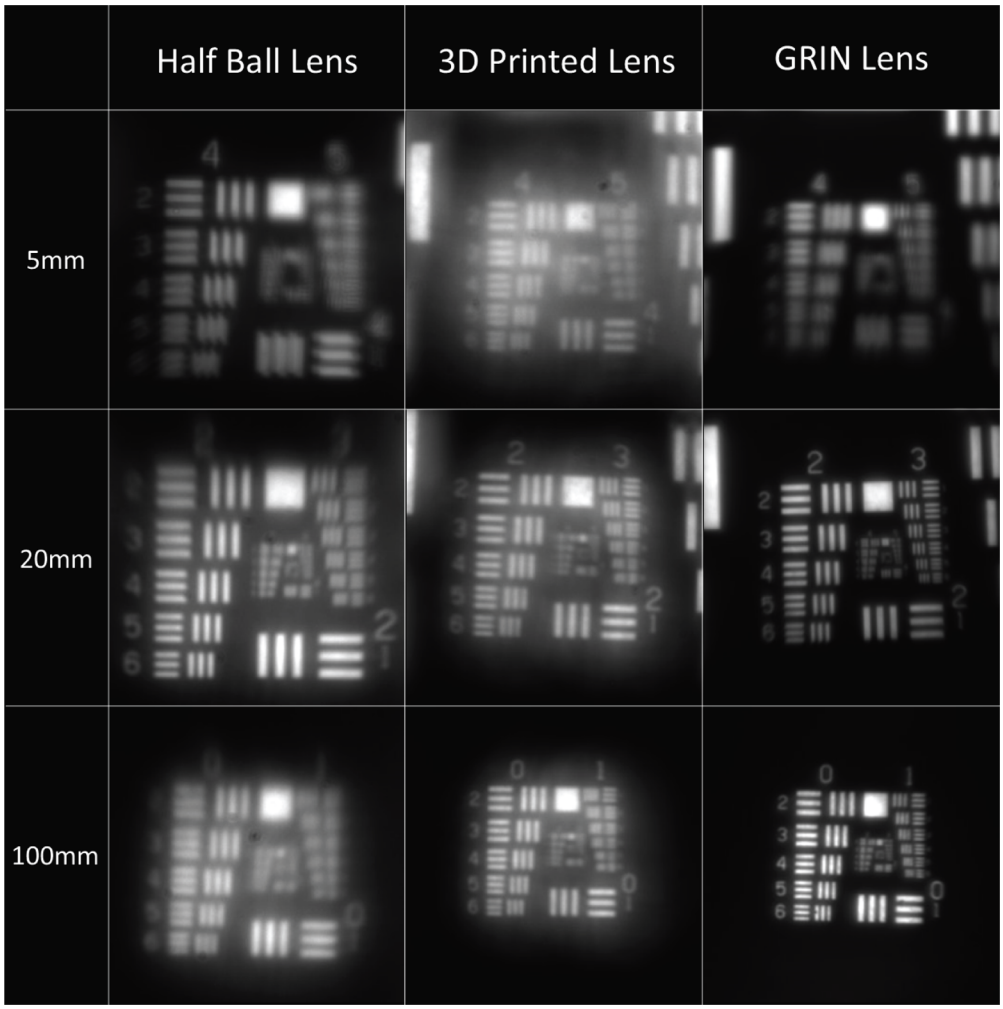

Fig. 5. Images at object distances of 5mm, 20mm, and 100mm for each of the 3 lenses being tested.

OSA CONTINUUM

5.2. Resolution and field of view

The images of the USAF Resolution Target were analyzed in ImageJ (National Institutes of Health, USA). A vertical line was drawn across the largest element of horizontally oriented lines in the frame and an intensity profile along that line was plotted. The maximum intensity value of the center bar (I_{max}) and the average of the two minimum values of the dark bars on either side (I_{min}) were recorded. These numbers were used to calculate contrast using the following equation:

$$C = \frac{I_{max} - I_{min}}{I_{max} + I_{min}} . \tag{2}$$

The same procedure was repeated with smaller and smaller elements in the image until the contrast dropped below 5%. The same process was repeated by drawing a horizontal line across vertically oriented lines and plotting the intensity profile to get the maximum and minimum values. The smallest element in either orientation which had a contrast greater than 5% was considered the smallest resolvable element.

Figure 5 shows images acquired during the experiment from 5mm, 20mm and 100mm object distances for each of the 3 lenses. These images were cropped to the same number of pixels (316 x 316) and contrast and brightness were adjusted only after analysis, for the purpose of visualization.

The image of the Ronchi Ruling was opened with Image J and a line was drawn perpendicular to the direction of the line pairs in the image. The intensity plot along this line was viewed, and the number of line pairs was counted.

The full field of view (FFOV) was determined using the following geometric equation:

$$\theta_{FFOV} = 2 * \theta_{FOV} = 2 * tan^{-1}(\frac{n * k}{2 * d}) . \tag{3}$$

Here, n is the number of line pairs counted in the image, k is a conversion factor for the size of a linepair from inches to millimeters, and d is the object distance in millimeters. The object distance was 20mm away and the Ronchi ruling was 25 lp/inch (k = 1.016 mm/lp).

Table 1 summarizes the results from each lens listing the smallest resolvable element in either the vertical or horizontal direction in lp/mm and FFOV in degrees.

Table 1. Summary of the angular field of view and the smallest resolvable element in lp/mm at 4 object distances for the half-ball lens, 3D printed lens, and GRIN lens.

	Half-ball	3D Print	GRIN
distance = 5mm	22.6	20.2	20.2
distance = 20mm	8.0	8.0	16.0
distance = 50mm	2.2	3.6	6.4
distance = 100mm	1.4	1.8	3.2
FFOV	36.7°	39.2°	41.7°

6. Discussion

The shape profile of the printed lens had an RMS shape error of less than 0.6μm from the nominal design. While this current iteration does not provide superior imaging performance than the GRIN lens, it does have potential for future improvement. By optimizing print conditions for better optical surface quality, better quality images may be obtained. Additional optical surfaces may be incorporated into the print design for further image quality improvement. There may be some bulk scattering causing a foggy appearance to the images due to the optical properties of the resin. Print materials with better optical transparency could also improve image quality.

OSA CONTINUUM

Surface roughness and the corresponding image quality was not consistent between prints. This could be related to the storage conditions of the resin, printer environment, or other unidentified factors. Further studies to improve the optical surface quality related to these factors are warranted. Once optimized, reproducibility testing could be done to obtain an estimate of the variance expected from the prints. This could then be incorporated into the tolerancing of a design to ensure that the printer is capable of meeting the optical requirements for the system.

Optomechanical alignment of multiple glass lens elements on this scale is not practical as static cling makes any precision control nearly impossible. Being able to incorporate mechanical structures between lens elements during the production of the lens provides more flexibility during optical design than has been previously available.

Additive manufacturing gives a lens designer full freedom over the shape, making complex freeform shapes without symmetry possible. This feature could be utilized in other areas of optics such as illumination design [12]. As seen here, the ability to form an image with the 3D printed optic throughout a specified depth of focus, suggests using this technology in sub-millimeter endoscope designs is feasible.

Funding

National Institutes of Health (5 T32 EB000809-15); U.S. Department of Defense (W81XWH1810371).

Acknowledgments

We would like to thank Jude Coompson and Dr. Hao Xin for assistance with the use of the Photonic Professional 3D printer, David Vega for connecting us with NanoScribe for troubleshooting, and Dominique Galvez for assistance with the graphics in this publication.

Disclosures

The authors declare that there are no conflicts of interest related to this article.

References

1. X. Ouyang, Z. Yin, J. Wu, C. Zhou, and A. P. Zhang, "Rapid optical μ-printing of polymer top-lensed microlens array," Opt. Express **27**(13), 18376–18382 (2019).
2. W. Moench and H. Zappe, "Fabrication and testing of micro-lens arrays by all-liquid techniques," J. Opt. A: Pure Appl. Opt. **6**(4), 330–337 (2004).
3. C. Pan, T. Wu, M. Chen, Y. Chang, C. Lee, and J. Huang, "Hot embossing of micro-lens array on bulk metallic glass," Sens. Actuators, A **141**(2), 422–431 (2008).
4. L. Y. Lin, S. S. Lee, K. S. J. Pister, and M. C. Wu, "Micro-machined three-dimensional micro-optics for integrated free-space optical system," IEEE Photonics Technol. Lett. **6**(12), 1445–1447 (1994).
5. W. R. Cox, D. J. Hayes, T. Chen, D. W. Ussery, D. L. MacFarlane, and E. Wilson, "Fabrication of micro-optics by microjet printing," (1995).
6. Y.-L. Sung, J. Jeang, C.-H. Lee, and W.-C. Shih, "Fabricating optical lenses by inkjet printing and heat-assisted in situ curing of polydimethylsiloxane for smartphone microscopy," J. Biomed. Opt. **20**(4), 047005 (2015).
7. X. Lu and L. S. Khim, "A statistical experimental study of the injection molding of optical lenses," J. Mater. Process. Technol. **113**(1-3), 189–195 (2001). 5th Asia Pacific conference on Materials processing.
8. X. Chen, W. Liu, B. Dong, J. Lee, H. O. T. Ware, H. F. Zhang, and C. Sun, "High-speed 3d printing of millimeter-size customized aspheric imaging lenses with sub 7 nm surface roughness," Adv. Mater. **30**(18), 1705683 (2018).
9. T. Gissibl, S. Thiele, A. Herkommer, and H. Giessen, "Two-photon direct laser writing of ultracompact multi-lens objectives," Nat. Photonics **10**(8), 554–560 (2016).
10. T. Gissibl, S. Thiele, A. Herkommer, and H. Giessen, "Sub-micrometre accurate free-form optics by three-dimensional printing on single-mode fibres," Nat. Commun. **7**(1), 11763 (2016).
11. J. Greivenkamp, *Field Gide to Geometrical Optics* (SPIE Press, Bellingham, WA, 2004), third printing ed.
12. B. Assefa, T. Saastamoinen, M. Pekkarinen, V. Nissinen, J. Biskop, M. Kuittinen, J. Turunen, and J. Saarinen, "Realizing freeform lenses using an optics 3d-printer for industrial based tailored irradiance distribution," OSA Continuum **2**(3), 690–702 (2019).

155.54.15.182 {ts '2020-01-15 04:27:20'}